Influence of the layered silicate type on the structure, morphology and properties of cellulose acetate nanocomposites

Article *in* Cellulose · April 2012

DOI: 10.1007/s10570-012-9846-6

CITATIONS
16

READS
119

5 authors, including:

Rafaelle Romero
Federal University of Technology - Paraná/Brazil (UTFPR)
6 PUBLICATIONS **154** CITATIONS
SEE PROFILE

R.M.V. Alves
Instituto de Tecnologia de Alimentos
42 PUBLICATIONS **599** CITATIONS
SEE PROFILE

Maria Do Carmo Gonçalves
University of Campinas
124 PUBLICATIONS **2,713** CITATIONS
SEE PROFILE

Cellulose
DOI 10.1007/s10570-012-9846-6

ORIGINAL PAPER

Influence of the layered silicate type on the structure, morphology and properties of cellulose acetate nanocomposites

Rafaelle Bonzanini Romero · Marcia Maria Favaro Ferrarezi · Carlos Alberto Paula Leite · Rosa Maria Vercelino Alves · Maria do Carmo Gonçalves

Received: 15 August 2012 / Accepted: 10 December 2012

Abstract This paper deals with the effect of different montmorillonite source clays, including pristine and organophilic montmorillonites, on the structure, morphology and properties of cellulose acetate (CA)/clay nanocomposites. In this study, the nanocomposites were prepared by melt extrusion in the presence of the environmentally friendly triethyl citrate plasticizer. The structure and morphology of the materials were analysed by X-ray diffraction and scattering (SAXS), X-ray microtomography and energy filtered transmission electron microscopy (EFTEM). SAXS and EFTEM results indicated that the nanocomposite morphologies were made up of tactoids together with exfoliated clay platelets in different proportions depending on the clay type. It can be concluded that well distributed clay tactoids and platelets can be achieved in CA nanocomposites prepared by melt extrusion and consequently property improvements can be found by using pristine or organophilic clays. In this case, the addition of a plasticizer, able to intercalate in the clay gallery, seems to be sufficient to promote the clay delamination mechanism under shearing inside the cellulose acetate matrix.

Keywords Cellulose acetate · Nanocomposite · Layered silicate · Morphology · Mechanical and permeation properties

R. B. Romero · M. M. F. Ferrarezi · C. A. P. Leite · M. C. Gonçalves (✉)
Institute of Chemistry, University of Campinas (UNICAMP), P.O. Box 6154, Campinas, SP 13083-970, Brazil
e-mail: maria@iqm.unicamp.br

R. M. V. Alves
Packaging Technology Center (CETEA), P.O. Box 139, Campinas, SP 13070-178, Brazil

Introduction

Biopolymers have been in focus in the last decade in both scientific and commercial fields as an interesting alternative to replace conventional petroleum-based plastics, due to cellulose derivatives being an important class of biopolymers. Cellulose derivatives are applied in diverse areas, such as laminates, optical films, membrane and encapsulation applications, textile fibers and coatings for pharmaceuticals and foods (Edgar et al. 2001). Cellulose acetate (CA) is the most commercially applied cellulose ester derivative; its global production was over 800,000 metric tons in 2008 (Puls et al. 2011). Cellulose acetate presents high optical clarity and stiffness, but it is moisture sensitive, brittle and presents low dimensional stability under high temperature and humidity.

The common approach to enhance polymeric properties is the preparation of multiphase materials, e.g., blends and composites. Cellulose acetate/plant-based filler composites have been studied due to the structural similarity between the components, which

Published online: 21 December 2012

give good interfacial adhesion (Bledzki et al. 1996; Edgar et al. 2001; Gutierrez et al. 2012; Huber et al. 2012; Mohanty et al. 2004). However, when these composites are prepared by extrusion, the processing temperature is around the lignocellulosic fiber degradation temperature (Gutierrez et al. 2012). Thus, the substitution of cellulose fibers by inorganic fillers, such as layered silicates, is proposed to reduce the negative effect of process temperature on the composite structure.

Some studies of CA/layered silicate nanocomposites have been found in literature in the last 10 years, aiming, mainly, at the obtainment of physical property enhancements at low filler levels (de Lima et al. 2012a, b; Hassan-Nejad et al. 2009; Park et al. 2004a, b, 2006; Ray and Bousmina 2005; Rodriguez et al. 2012; Romero et al. 2009; Wibowo et al. 2006; Yoshioka et al. 2006). Romero et al. (2009) prepared CA/pristine montmorillonite (MMT) nanocomposites by solution intercalation process, using acetone, acetic acid, acetone/water and acetic acid/water solutions. The nanocomposites prepared in acetic acid/water solution showed the highest clay delamination, probably due to the high polarity of the solvents and the formation of hydrogen bonds with the layered silicate platelets, showing that pristine MMT exfoliation can easily be achieved by solution intercalation method, when CA is used as the polymeric matrix. However, it should be taken into consideration that pristine silicate layers are hydrophilic, which can hinder the filler effective intercalation and distribution throughout hydrophobic matrices by other intercalation methods, such as melt intercalation. In these cases, the cations present in the clay interlayer gallery are usually substituted by quaternized ammonium or phosphonium cations to produce organophilic clays (Ray and Bousmina 2005).

Literature results (Alexandre and Dubois 2000; Li and Ishida 2003; Ray and Bousmina 2005; Romero et al. 2009) show that good control of the nanocomposite structure can be achieved by the solution intercalation method; however, the melt intercalation method is particularly interesting due to its easy adequation to conventional industrial processes (Alexandre and Dubois 2000; Ray and Bousmina 2005; Shen et al. 2002). Therefore, the investigation of the melt intercalation method must be made in order to achieve the adequate filler dispersion and distribution in polymer matrices.

Cellulose acetate can only be satisfactory melt processed in the presence of a plasticizer, as the process temperature can exceed the CA degradation onset temperature. Phthalate derivatives are widely used as cellulose derivative plasticizers (Crawford and Esmerian 2006; Park et al. 2004a, b; Yamaguchi et al. 2009), however, these reagents are toxic and potentially carcinogenic. The research herewith is targeted at using a suitable environmentally friendly plasticizer in formulating CA nanocomposites. Citric acid esters are nontoxic and have been approved for several applications such as additives for medical plastics, personal care and food contact (Bodmeier and Paeratakul 1994; Johnson 2002). Park et al. (2004a, b) prepared CA/organophilic montmorillonite (MMTO) nanocomposites by melt intercalation process using triethyl citrate (TEC) as a plasticizer. The nanocomposites exhibited lower vapor permeability properties than pure CA. In a sequential study (Park et al. 2004a, b), the authors used maleic anhydride grafted cellulose acetate butyrate (CAB-*g*-MA) as a compatibilizer for CA/TEC/MMTO nanocomposites. The CAB-*g*-MA improves MMTO dispersion and consequently, CA mechanical properties. The highest mechanical property gains were obtained for the nanocomposites with exfoliated morphology, which is attained at 5 wt% CAB-*g*-MA. On the other hand, Yoshioka et al. (2006) prepared CA/clay/poly(ε-caprolactone) nanocomposites by in situ polymerization of poly(ε-caprolactone) in the presence of CA and using three layered silicate types: montmorillonite, hectorite and fluoromica modified with several kinds of ammonium salts. The authors showed that the interlayer silicate gallery distances were dependent on the number of hydroxyl groups of the organomodifier and that almost complete clay exfoliation was achieved in the presence of organomodifiers with two hydroxyl groups. The authors concluded that effective clay organic modification is needed in order to obtain desirable materials. In recent studies, de Lima et al. (2012a, b) also studied CA/MMTO nanocomposites obtained by melt intercalation method, using two different plasticizers: di-octyl phthalate (DOP) and TEC. The nanocomposites presented mixed morphologies with intercalated and exfoliated clay structures. CA mechanical properties were the same for both plasticizers. The authors confirmed that TEC can be an efficient CA plasticizer and can substitute DOP, as initially indicated by Park et al. (2004a, b).

The aim of this study is to investigate the structure, morphology and properties of CA/clay nanocomposites, obtained from different montmorillonite source clays, including pristine and organophilic montmorillonites with different cationic exchange capacity. Several works in literature (Okada and Usuki 1995; Yilmaz et al. 2010) have shown results about the influence of clay type on nanocomposite properties for different polymer matrixes (nylon 6, vulcanized rubber, poly(ethylene terephthalate), acrylic terpolymer) and using different preparation techniques. The results showed that although the final morphologies and properties of the nanocomposites were dependent on the polymeric matrix and clay, the effect of the clay type cannot be generalized. In the study herewith, it will be shown that well dispersed clay platelets can be achieved in CA nanocomposites prepared by melt extrusion either by using organophilic or pristine clay. To do so, the cellulose acetate nanocomposites were prepared by melt intercalation method using the environmentally friendly triethyl citrate plasticizer to improve the processability of CA. The material characterization was carried out with X-ray diffraction and low angle X-ray scattering; X-ray microtomography and energy filtered transmission electron microscopy. Also, tension, flexural and water vapour permeation properties were evaluated.

Experimental

Materials

Cellulose acetate (CA) with 39.8 wt% acetyl content, 2.45 substitution degree and number-average molecular mass of 50,000 g mol^{-1} was purchased from Eastman Chemicals Co. Triethyl citrate (TEC) was purchased from Acros Organics.

Four different layered silicates were used: (1) a pristine sodium montmorillonite (MMT-P) supplied by Eduardo Vasconcelos Representações Ltda (Porto Alegre, Brazil); (2) a pristine sodium montmorillonite (MMT-CNa) purchased from Southern Clay Products (TX, USA); (3) a long chain quaternary alkyl ammonium salt chemically modified montmorillonite (MMTO-V) purchased from Bentec (Livorno, Italy); and (4) a methyl tallow bis-2-hydroxyethyl quaternary ammonium montmorillonite (MMTO-C30B) purchased from Southern Clay Products (Texas, USA). Table 1 shows some characteristics of the clays given by the suppliers.

Table 1 Clay properties given by the suppliers

Clays	Commercial designation	Cationic exchange capacity (meq 100 g^{-1})	Dry particle size (microns by volume)
MMT-P	Polenita	62	–[a]
MMT-CNa	Cloisite® Na^+	92	90 % less than 13 μm
MMTO-V	Viscogel ED	–[a]	76 μm
MMTO-C30B	Cloisite® 30B	90	90 % less than 13 μm

[a] Values not given by the suppliers

Melt processing of the CA nanocomposites

Cellulose acetate (CA) and layered silicate powders were dried under vacuum at 80 °C for 24 h before use. TEC was used in the preparation of CA nanocomposites as a plasticizer, facilitating CA melt processing, and as clay expansor, since the hydroxyl and carbonyl groups present in the TEC structure can interact with the pristine clay surface or with a suitable organic modifier present in the clay gallery.

Each layered silicate was mechanically pre-mixed with TEC in a laboratory blender waring commercial® during 5 min. The TEC/layered silicate mixture was then mixed with CA. The nanocomposites were prepared with 20 wt% TEC and 5 wt% clay in relation to the CA weight. The materials were processed in a APV 2000 co-rotational twin screw extruder (with a L/D ratio of 13) at 190–220 °C temperature range and 100–125 rpm rotation range. The extruded nanocomposite pellets were dried and then injection molded into standard tensile (ASTM D638) and flexural (ASTM D790) specimens in an Arburg Allrounder 221 M 250-55 injection molding machine at 190–220 °C temperature range, 40 °C mold temperature, 1,100 bar injection pressure and 650 bar holding pressure.

Characterization of the materials

X-ray diffraction (XRD) measurements were carried out using a Shimadzu XRD-7,000 diffractometer in the reflection mode with an incident Cu-Kα radiation

($\lambda = 0.1540$ nm) under a 0.5° min^{-1} scan rate. The X-ray scattering experiments were carried out at the D11A-SAXS1 beamline of the National Synchrotron Light Laboratory (Campinas, Brazil). A two-dimensional position sensitive detector with a 477.5 mm sample-to-detector distance and a 0.1608 nm wavelength was used. The measurements were obtained at 25 °C. Parasitic scattering was subtracted from the total intensity and the scattering profiles were corrected for sample absorption and detector response. The X-ray microtomograph analysis were carried out in a desktop X-ray micro-CT scanner equipment (SkyScan 1074, Aartselaar, Belgium) equipped with a 768 × 576 pixel 8-bit X-ray camera in on-chip integration mode with lens coupled to a scintillator (30 μm of resolution). A CA/TEC film was layered over each nanocomposite film prior to imaging as reference.

The morphology and the silicon and carbon elemental distributions in the nanocomposites were examined in a Carl Zeiss CEM 902 transmission electron microscope associated to electron energy loss spectroscopy elemental mapping. The microscope was operated at an acceleration voltage of 80 kV equipped with a Castaing–Henry energy filter spectrometer within the column. Ultrathin sections, approximately 40 nm thick, were cut at −100 °C, in a Leica EM FC6 cryo-ultramicrotome. Elemental images were obtained for silicon (Si) and carbon (C) using the three-window method. The energy-selecting slit was set at 132 eV for Si and 303 eV for C, with a 20 eV energy slit width. The images were recorded using a slow-scan CCD camera (Proscan) and processed using the Universal Imaging Platform (iTEM) software.

Tensile and flexural tests were performed according to ASTM D638 and ASTM D790 standards, respectively, using an EMIC DL2000 universal testing machine. Seven injection-molded specimens were tested for each sample and the reported values are the calculated averages.

The water vapour permeation rate of the materials was determined by the gravimetric method according to ASTM E96/E96 M-05. This methodology is based on the mass increase of anhydride calcium chloride placed inside an aluminium capsule coated with the sample film. The analyses were carried out in a controlled temperature and humidity environment at the laboratory of the Packaging Technology Center of the Institute of Food Technology—CETEA/ITAL (Campinas, Brazil). Sample films with an approximate 388 μm thickness were obtained for these analyses by compression molding process using the extruded materials. At least five specimens of each material were measured.

Results and discussion

The nanocomposites were first investigated by X-ray microtomography, which can give a macroscopic visual overview of the clay distribution level throughout the matrix. In this technique, the image contrast is formed due to X-ray absorption in different areas of the sample, which is a function of its density and atomic mass; therefore, the sample internal structure can be analysed without carrying out laborious sample preparation. Figure 1 shows the X-ray microtomographic images along with the linescan plots measured along the stripes. The CA/TEC/MMT-P sample presented the most non-uniform color-level image among the samples. A uniform color-level profile indicates better clay distribution. Thus, CA/TEC/MMT-P nanocomposite probably presented large clay agglomerates throughout the matrix, while CA/TEC/MMT-CNa, CA/TEC/MMTO-V and CA/TEC/MMT-C30B profiles indicate a good clay dispersion level. The sample line-profile scan also indicates the filler distribution level. Peak absence indicates a more uniform particle distribution. Therefore, CA/TEC/MMT-P presented the worst MMT distribution level. In addition, the results indicated that the shearing promoted during the processing was efficient in the distribution of clay particles, suggesting that the previously swollen clay particles with the TEC plasticizer facilitated the breaking of the aggregates. The swelling effect of the plasticizer on the clay structure can be better investigated by XRD.

The X-ray diffraction patterns of the layered silicates and CA nanocomposites are presented in Fig. 2. The (001) reflection peaks for the original clays were shifted to lower values for all clays after TEC addition; gallery distances increased from 1.2 to 1.6 nm (TEC/MMT-P), from 1.1 to 3.7 nm (TEC/MMT-CNa), from 3.3 to 3.5 nm (TEC/MMTO-V) and from 1.8 to 3.8 nm (TEC/MMTO-C30B). These results indicate that TEC molecules were able to penetrate the clay interlayer gallery, reducing the attractive forces between the charged layer surfaces

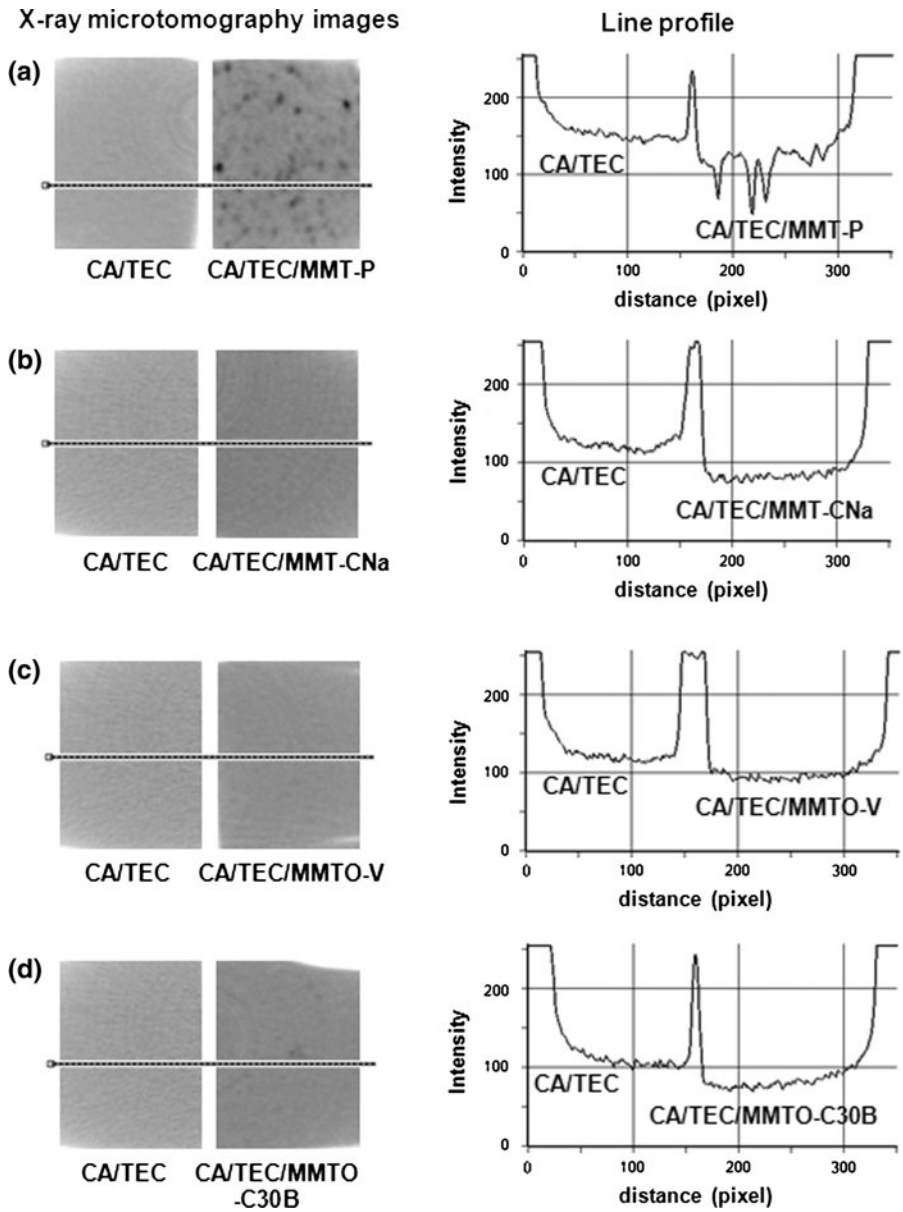

Fig. 1 X-ray microtomography images and line profiles of the nanocomposites: **a** CA/TEC/MMT-P, **b** CA/TEC/MMT-CNa, **c** CA/TEC/MMTO-V and **d** CA/TEC/MMTO-C30B

and the counterions, consequently leading to layer separation. The low increase obtained for the MMTO-V clay is probably due to the already large distance between the layers of this specific silicate. It is noteworthy that besides the main reflection peaks of TEC/MMT-CNa and TEC/MMTO-C30B, a second and third harmonics of the first reflection became more evident. These results reveal uniform intercalation of TEC chains into the interlayer region of the clays, resulting in the maintenance or even increase in the stacking order of the clay gallery.

The nanocomposite diffractograms (Fig. 2) showed that all CA nanocomposites developed intercalated structures. The calculated clay gallery distances were 1.6, 1.7, 3.2 and 2.9 nm for the CA/TEC/MMT-P, CA/TEC/MMT-CNa, CA/TEC/MMTO-V and CA/TEC/MMTO-C30B, respectively. A slight decrease of the gallery distance was obtained for CA/TEC/MMTO-V compared to TEC/MMTO-V, which could be associated to the collapse of MMT platelets during processing due to the partial extraction of the clay surfactant or the intercalated TEC plasticizer at the

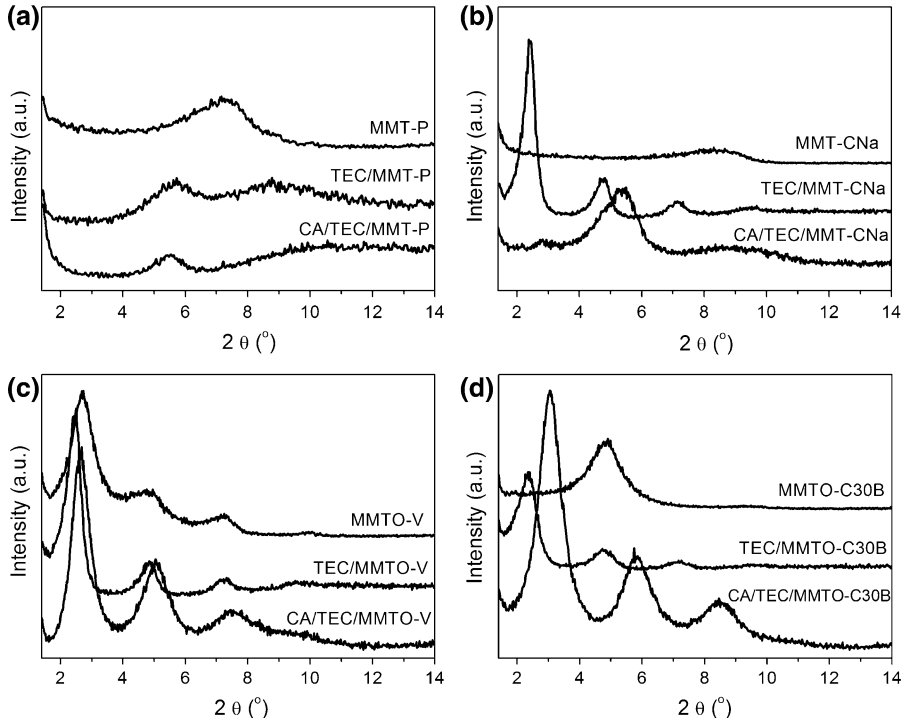

Fig. 2 X-ray diffraction results of the layered silicates, TEC/layered silicate and CA/TEC nanocomposites with: **a** MMT-P, **b** MMT-CNa, **c** MMTO-V and **d** MMTO-C30B

extrusion process temperature. On the other hand, significant decreases were observed for the gallery distances for the CA/TEC/MMT-CNa and CA/TEC/MMTO-C30B nanocomposites when compared to TEC/MMT-CNa and TEC/MMTO-C30B samples, which could be due to a certain TEC migration from the clay gallery to the CA matrix. Apart from this, an interdiffusion process between TEC and CA chains could also have occurred in these materials during the melt processing, if the resulting loss of conformational entropy of the confined CA polymer chains could be driven by favorable interactions between CA groups, TEC groups, and clay surface groups.

2D-SAXS/WAXS analyses were carried out to complement the XRD results. The 2D-SAXS/WAXS technique is useful to determine both gallery distance and relative orientation of the layered silicate in a polymeric matrix. The low angle range evaluation is especially important to check the conditions in which the clay basal peaks disappear, which is considered an appropriate sign of exfoliation. Also, this technique allows the evaluation of the number of the stacked clay layers.

Figure 3 shows the Lorentz's corrected intensity (I(q)) as a function of the scattering vector (q) for the samples. The corresponding d-spacings of the nanocomposites obtained by SAXS technique show good agreement with the XRD results. From SAXS results, the calculated gallery distances of the nanocomposites were 1.6 nm (CA/TEC/MMT-P), 1.6 nm (CA/TEC/MMT-CNa), 3.5 nm (CA/TEC/MMTO-V) and 3.3 nm (CA/TEC/MMTO-C30B).

The analyses of the low angle region ($q < 1\ nm^{-1}$) can give extra information about the clay platelets. The curve at the initial region showed an angular dependence of q^{-3} for TEC/MMT-P and TEC/MMT-CNa samples, suggesting the presence of tactoids with different thickness, which interact between themselves developing curved and bent structures (fractal contribution to shape). On the other hand, TEC/MMTO-V and TEC/MMT-C30B showed an angular dependence of $q^{-2.5}$ and $q^{-2.8}$, respectively, indicating an intermediary state made up of individual clay lamellae and/or tactoids with different thicknesses. For all the CA/TEC/clay nanocomposites, the angular dependence was between $q^{-2.5}$ and $q^{-2.7}$, suggesting that the nanocomposite morphologies were made up of tactoids and delaminated lamellae.

In addition, for any periodic structure, the scattering pattern geometry reflects the extent of orientation of

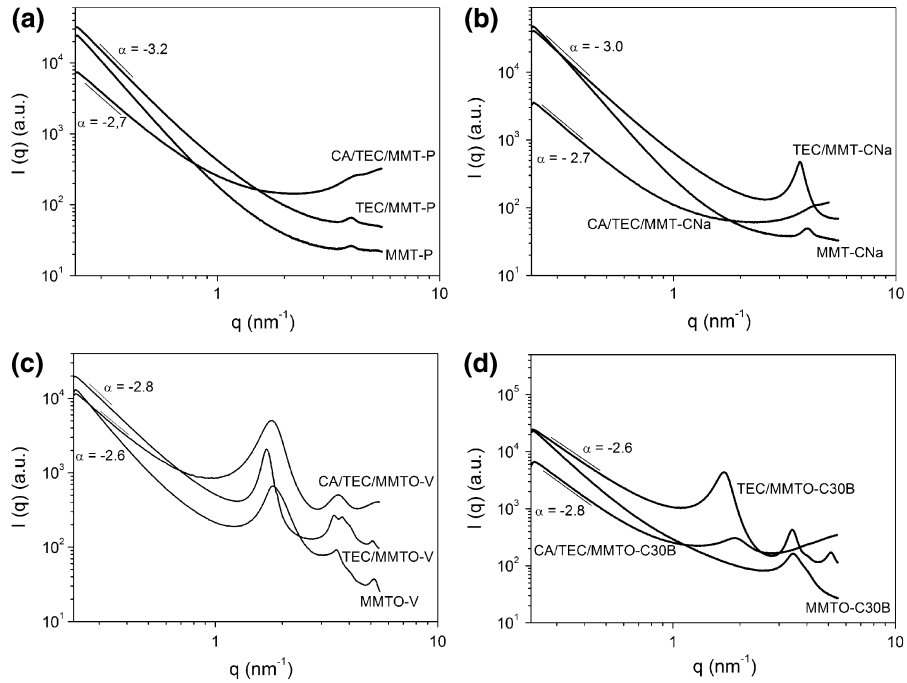

Fig. 3 SAXS results of the layered silicates, TEC/layered silicate and CA/TEC nanocomposites with: **a** MMT-P, **b** MMT-CNa, **c** MMTO-V and **d** MMTO-C30B

the stacked layers in the material. The 2D-SAXS patterns of the materials are shown in Fig. 4. An isotropic scattering pattern (perfect central rings) was observed for CA/TEC/MMT-P nanocomposite, suggesting that there was no preferential orientation of clay particles in this sample, and a slight anisotropic pattern was observed for CA/TEC/MMT-CNA nanocomposite. CA/TEC/MMTO-V and CA/TEC/MMTO-C30B presented typical patterns of anisotropic samples (central rings were deformed and acquired an elliptical shape). This elliptical shape is associated to filler preferential orientation throughout the matrix, favoured by shearing during processing, which causes crystallographic domain deformations along the macroscopic axis. As the samples were exposed to radiation at a perpendicular direction to the moulding plane, it is concluded that clay tactoids or clay lamellae were oriented along the injection flux direction.

The nanocomposite morphological characteristics were also investigated by transmission electron microscopy (TEM) (Fig. 5). CA/TEC/MMT-P and CA/TEC/MMT-CNa morphologies presented some tactoids together with individual lamellae. The clay particles in CA/TEC/MMT-P were 94 ± 84 nm (mean) long and 10 ± 4 nm (mean) thick, while the ones in CA/TEC/MMT-CNa were 117 ± 89 nm (mean) long and 3 ± 4 nm (mean) thick. Also, between these samples, the clay particles presented a higher exfoliation degree within the polymer matrix in the CA/TEC/MMT-CNa, as initially observed by the X-ray microtomography results, which is probably due to the higher TEC penetration level in the TEC/MMT-CNa sample than in the TEC/MMT-P, as observed by X-ray diffraction results.

CA/TEC/MMTO-V showed the presence of tactoids as well as partially exfoliated silicate platelets with preferential orientation, as previously observed by SAXS. The clay particles presented 154 ± 76 nm (mean) length and 5 ± 3 nm (mean) thickness. CA/TEC/MMTO-C30B nanocomposite showed a morphology formed by clay tactoids and exfoliated clay layers with 174 ± 78 nm (mean) length and 2 ± 1 nm (mean) thickness. Moreover, the insets in Fig. 5 present clay particles inside the CA matrix at higher magnification and show that the polymer and clay domains are well connected, shown by the integrity of the clay–polymer interfaces, even in the CA/TEC/MMT-P nanocomposite, which has a prevalence of tactoids (Fig. 5a).

The TEM micrographs showed better exfoliation and higher content of individual clay platelets for the

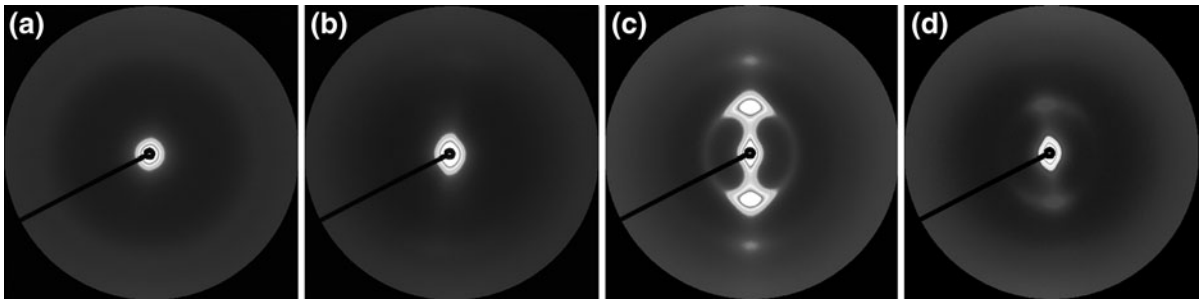

Fig. 4 2D-SAXS/WAXD patterns for the: **a** CA/TEC/MMT-P, **b** CA/TEC/MMT-CNa, **c** CA/TEC/MMTO-V and **d** CA/TEC/MMTO-C30B

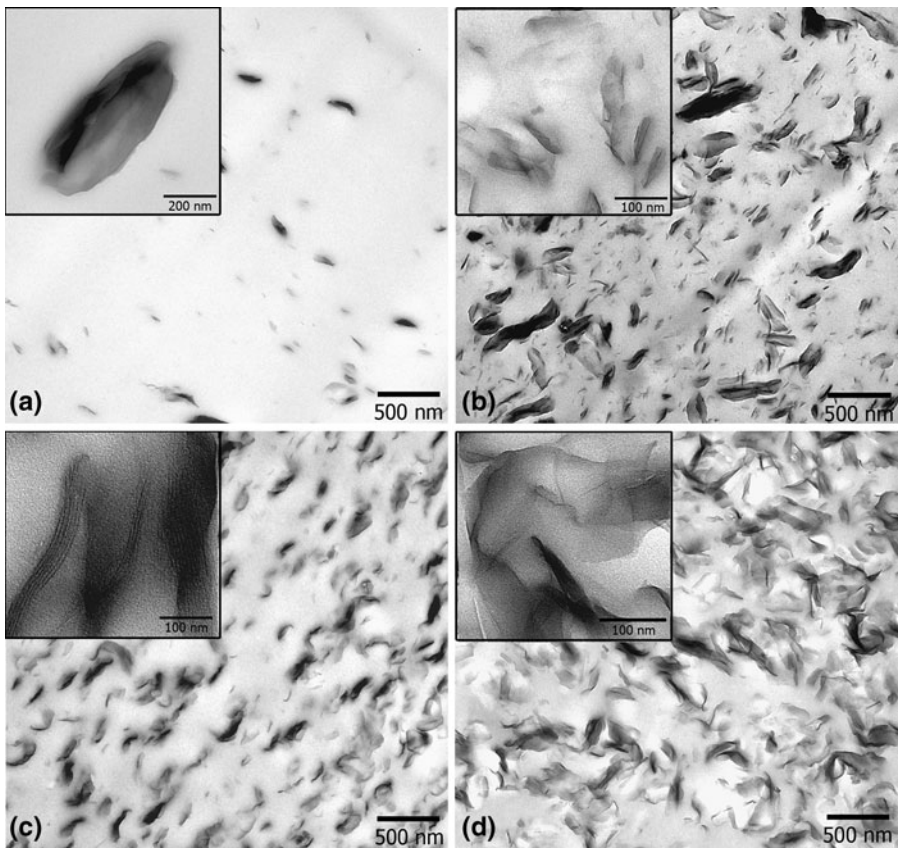

Fig. 5 TEM micrographs of the nanocomposites: **a** CA/TEC/MMT-P, **b** CA/TEC/MMT-CNa, **c** CA/TEC/MMTO-V and **d** CA/TEC/MMTO-C30B

CA/TEC/MMTO-C30B compared to the CA/TEC/MMTO-V. This difference may be due to higher intercalation of TEC molecules in the MMTO-C30B clay gallery compared to the MMTO-V clay. The hydroxy-ethyl groups of the organic modifier in the MMTO-C30B can interact more readily with the hydroxyl groups of the triethyl citrate (TEC) plasticizer and consequently the CA/TEC mixture can intercalate more effectively in the clay gallery. In addition, increasing the number of direct CA/TEC-organoclay contacts ultimately leads to an increase in the level of platelet exfoliation (Fornes et al. 2002). Comparing the SAXS with the TEM results, it is possible to state that the SAXS results are coherent

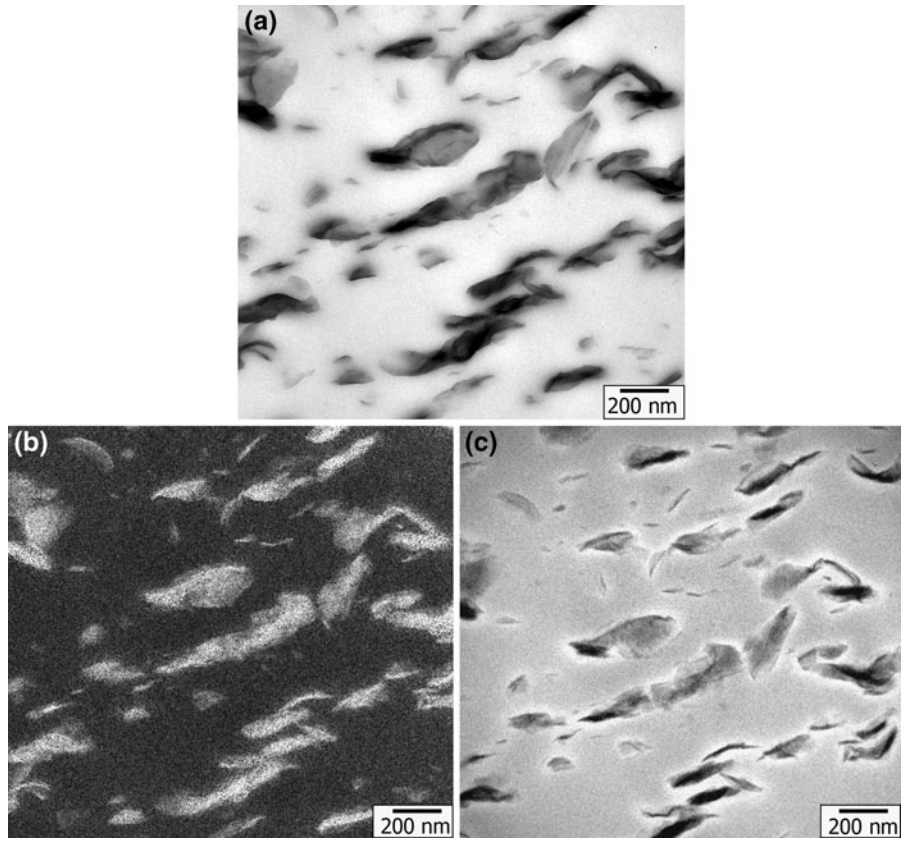

Fig. 6 EFTEM images of the CA/TEC/MMTO-V nanocomposites **a** bright field, **b** silicon map and **c** carbon map

with the TEM images which showed that the CA/TEC/MMT-CNa, CA/TEC/MMTO-V and CA/TEC/MMTO-C30B nanocomposite clays presented the highest delamination and that the CA/TEC/MMTO-V nanocomposite showed the highest orientation.

Moreover, for the CA/TEC/MMTO-C30B nanocomposite, the TEM images showed that the clay platelets were not totally oriented in a preferred direction. In fact, they are randomly dispersed, but associated in large groups, suggesting the formation of large tridimensional structures, named "castle of cards". Ren et al. (2000) proposed a model to explain the formation of these specific tridimensional structures, in which the "castle of cards" is composed of stacks of dozens of individual lamellae. Also, in this model the dispersed tactoids presented an anisotropic aspect and were percolated, which prevented the free individual rotation and relaxation phenomena.

Besides, considering the clay gallery distance calculated by XRD and the clay particle thickness dimensions determined by TEM in all nanocomposites, it is possible to conclude that the layered silicates dispersed in the CA matrix were in the range of individual lamellae and aggregates which were made up of 13 clay lamellae in average.

Elemental analysis associated with transmission electron microscopy is an interesting technique to visualize phase arrays in blends and composites as each component generates different spectrum in the low-energy-loss region, allowing for the visualization of phases, even of compounds of the same elements. In this work, elemental analyses of carbon and silicon were carried out in order to better evaluate the spatial distribution of clay particles, more specifically the exfoliated clay platelets, which can present insufficient contrast at conventional bright field TEM images. Figures 6 and 7 show the bright-field images and elemental maps of Si and C for CA/TEC/MMTO-V and CA/TEC/MMT-CNa nanocomposites. In the bright field images (Figs. 6a, 7a), the dark regions are

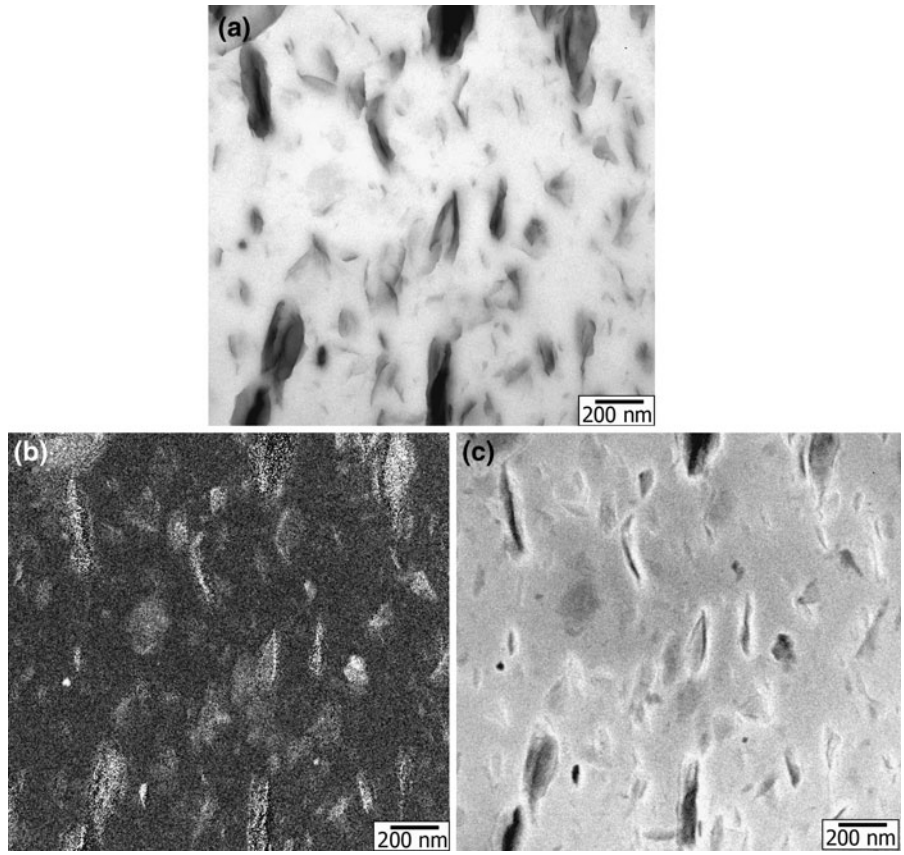

Fig. 7 EFTEM images of the CA/TEC/MMT-CNa nanocomposites **a** bright field, **b** silicon map and **c** carbon map

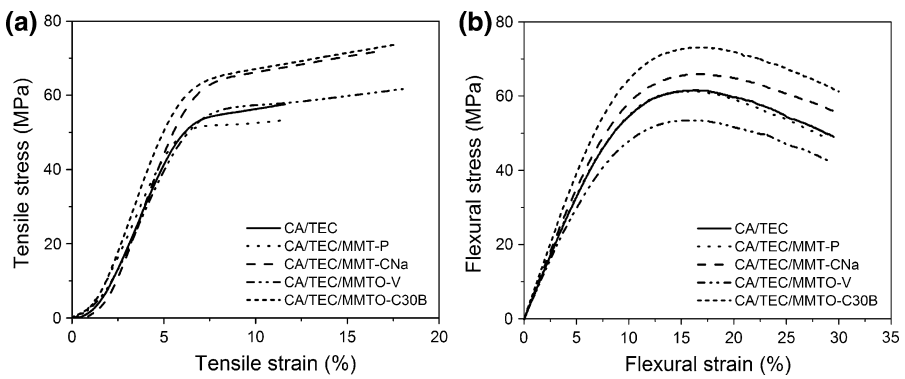

Fig. 8 Mechanical results of the CA/TEC and nanocomposites **a** tensile and **b** flexural tests

related to the denser phase, i.e., the silicate platelets, and correspond to the white regions in the silicon mapping (Figs. 6b, 7b) of the same area. The silicon elemental maps confirm that the clay platelet arrangements are formed by a roughly regularly spaced and relatively curved array of platelets in the cellulose acetate film. On the other hand, the bright regions in Figs. 6c and 7c represent carbon-rich regions. These carbon maps also show the exfoliated clay platelets but reveal a carbon-rich layer

Table 2 Mechanical properties and water vapour transmission rate (WVTR) of the CA/TEC and nanocomposites

Samples	Tensile strength (MPa)	Young's modulus (MPa)	Elongation at break (%)	Flexural strength (MPa)	Flexural modulus (MPa)	WVTR (g_{water}/m^2 day)
CA/TEC	60 ± 1	1375 ± 20	13 ± 1	60 ± 1	3295 ± 100	130 ± 1
CA/TEC/MMT-P	54 ± 2	1355 ± 60	11 ± 1	61 ± 1	3395 ± 70	124 ± 5
CA/TEC/MMT-CNa	72 ± 2	1530 ± 65	15 ± 1	67 ± 1	3680 ± 160	90 ± 9
CA/TEC/MMTO-V	60 ± 2	1275 ± 25	16 ± 1	52 ± 1	3080 ± 40	97 ± 7
CA/TEC/MMTO-C30B	73 ± 1	1570 ± 47	16 ± 1	69 ± 1	4182 ± 100	88 ± 3

surrounding and penetrating the clay particles, which suggests a high concentration of surfactant and/or plasticizer at the clay/polymer interface.

Lastly, the mechanical and permeability properties of the CA nanocomposites were evaluated. The mechanical results are shown in Fig. 8 and summarized in Table 2. These results showed that CA/TEC/MMT-CNa and CA/TEC/MMT-C30B presented higher elastic and flexural modulus and higher tensile and flexible strength than CA/TEC. On the other hand, CA/TEC/MMT-P and CA/TEC/MMTO-V presented no enhancement of these mechanical properties when compared to the CA/TEC sample. Based on SAXS results and TEM images, it can be seen that the polymer and clay domains were well connected suggesting that the hydroxyl and carbonyl groups present in the TEC structure as well as the hydroxyl and acetyl groups in cellulose acetate can interact with the structural oxygen and the Si–OH groups from the pristine clay or with a suitable organic modifier present in the clay gallery. Moreover, the nanocomposites presented a slightly higher elongation at break than CA/TEC, which could be due to better stress absorption by the high dispersed clay platelets as well as to the possible concentration of surfactant and plasticizer molecules at the matrix/clay interface, which could decrease the friction between CA chains and clay platelets. Apart from this, CA/TEC/MMTO-30B was the nanocomposite which presented the best mechanical properties due probably to the better dispersion and arrangement of the clay particles in the polymer matrix, as observed by TEM.

The permeability results showed decreases in the cellulose acetate water vapour transmission rate (WVTR) with the addition of the layered silicates. CA/TEC presented a WVTR value of 130 ± 1 g_{water}/m^2 day at 38 °C and 90 % RH, while the WVTR values for the CA nanocomposites were 124 ± 5, 90 ± 9, 97 ± 7 and 88 ± 3 g_{water}/m^2 day for CA/TEC/MMT-P, CA/TEC/MMT-CNa, CA/TEC/MMTO-V and CA/TEC/MMTO-C30B, respectively. These results are attributed to the good clay dispersion and distribution throughout the CA matrix.

Based on the findings reported in this study, it is possible to conclude that well dispersed clay platelets can be achieved in CA nanocomposites prepared by melt extrusion and consequently property improvements can be found even without using surfactant pretreated clay. In this case, the addition of a plasticizer, able to intercalate in the clay gallery, seems to be sufficient to initiate the clay delamination mechanism under shearing inside the cellulose acetate matrix.

Conclusion

The results indicated that besides TEC being used as CA plasticizer, facilitating the CA melt processing, it also intercalated in the clay interlayer region and eventually facilitated clay exfoliation during the melt processing. SAXS and EFTEM results suggested that the nanocomposite morphologies were composed of tactoids and delaminated lamellae. Lastly, the better dispersion and property enhancement were obtained using pristine montmorillonite (MMT-CNa) and organophilic montmorillonite (MMTO-C30B). Thus, the herewith applied methodology showed that CA properties, such as tensile strength and water vapour permeation, can be optimized even by the addition of pristine layered silicates.

Acknowledgments This research was supported by Coordenação de Aperfeiçoamento de Pessoal de Nível Superior (CAPES), Conselho Nacional de Desenvolvimento

Científico e Tecnológico (CNPq) and Fundação de Amparo à Pesquisa do Estado de São Paulo (FAPESP) (Brazil).

References

Alexandre M, Dubois P (2000) Polymer-layered silicate nanocomposites: preparation, properties and uses of a new class of materials. Mater Sci Eng 28:1–63

Bledzki AK, Reihmane S, Gassan J (1996) Properties and modification methods for vegetable fibers for natural fiber composites. J Appl Polym Sci 59:1329–1336

Bodmeier R, Paeratakul O (1994) The distribution of plasticizers between aqueous and polymer phases in aqueous colloidal polymer dispersions. Int J Pharm 103:41–54

Crawford RR, Esmerian OK (2006) Effect of plasticizers on some physical properties of cellulose acetate phthalate films. J Pharm Sci 60:312–314

de Lima JA, Pinotti CA, Felisberti MI, Gonçalves MC (2012a) Morphology and mechanical properties of nanocomposites of cellulose acetate and organic montmorillonite prepared with different plasticizers. J Appl Polym Sci 124:4628–4635

de Lima JA, Pinotti CA, Felisberti MI, Gonçalves MC (2012b) Blends and clay nanocomposites of cellulose acetate and poly (epichlorohydrin). Comp Part B 43:2375–2381

Edgar KJ, Buchanan CM, Debenham JS, Rundquist PA, Seiler BD, Shelton MC, Tindall D (2001) Advances in cellulose ester performance and application. Prog Polym Sci 26: 1605–1688

Fornes TD, Yoon PJ, Hunter DL, Keskkula H, Paul DR (2002) Effect of organoclay structure on nylon 6 nanocomposites morphology and properties. Polymer 43:5915–5933

Gutierrez MC, De Paoli M-A, Felisberti MI (2012) Biocomposites based on cellulose acetate and short curauá fibers: effect of plasticizers and chemical treatments of the fibers. Compos Part A 43:1338–1346

Hassan-Nejad M, Ganster J, Bohn A, Pinnow M, Volker B (2009) Bio-based nanocomposites of cellulose acetate and nano-clay with superior mechanical properties macromol. Symp 280:123–129

Huber T, Müssig J, Curnow O, Pang S, Bickerton S, Staiger MP (2012) A critical review of all-cellulose composites. J Mater Sci 47:1171–1186

Johnson W Jr (2002) Final report on the safety assessment of acetyl triethyl citrate, acetyl tributyl citrate, acetyl trihexyl citrate, and acetyl trioctyl citrate. Int J Toxicol 21(Suppl 2):1–17

Li Y, Ishida H (2003) Solution intercalation of polystyrene and the comparison with poly(ethyl methacrylate). Polymer 44:6571–6577

Mohanty AK, Wibowo A, Misra M, Drzal LT (2004) Effect of process engineering on the performance of natural fiber reinforced cellulose acetate biocomposites. Compos Part A 35:363–370

Okada A, Usuki A (1995) The chemistry of polymer–clay hybrids. Mater Sci Eng C3:109–115

Park H-M, Misra M, Drzal LT, Mohanty AK (2004a) "Green" nanocomposites from cellulose acetate bioplastic and clay: effect of eco-friendly triethyl citrate plasticizer. Biomacromolecules 5:2281–2288

Park H-M, Liang X, Mohanty AK, Misra M, Drzal LT (2004b) Effect of compatibilizer on nanostructure of the biodegradable cellulose acetate/organoclay nanocomposites. Macromolecules 37:9076–9082

Park H-M, Mohanty AK, Drzal LT, Lee E, Mielewski DF, Misra M (2006) Effect of sequential mixing and compounding conditions on cellulose acetate/layered silicate nanocomposites. J Polym Environ 14:27–35

Puls J, Wilson SA, Hölter D (2011) Degradation of cellulose acetate-based materials: a review. J Polym Environ 19: 152–165

Ray SS, Bousmina M (2005) Biodegradable polymers and their layered silicate nanocomposites: in greening the 21st century materials world. Prog Mater Sci 50:962–1079

Ren J, Silva AS, Krishnamoorti R (2000) Linear viscoelasticity of disordered polystyrene–polyisoprene block copolymer based layered-silicate nanocomposites. Macromolecules 33:3739–3746

Rodriguez FJ, Galotto MJ, Guarda A, Bruna JE (2012) Modification of cellulose acetate films using nanofillers based on organoclays. J Food Eng 110:262–268

Romero RB, Leite CAP, Gonçalves MC (2009) The effect of the solvent on the morphology of cellulose acetate/montmorillonite nanocomposites. Polymer 50:161–170

Shen Z, Simon GP, Cheng Y-B (2002) Comparison of solution intercalation and melt intercalation of polymer–clay nanocomposites. Polymer 43:4251–4260

Wibowo AC, Misra M, Park H-M, Drzal LT, Schalek R, Mohanty AK (2006) Biodegradable nanocomposites from cellulose acetate: mechanical, morphological, and thermal properties. Comp Part A 37:1428–1433

Yamaguchi M, Iwasaki T, Okada K, Okamoto K (2009) Control of optical anisotropy of cellulose esters and their blends with plasticizer. Acta Mater 57:823–829

Yilmaz O, Cheaburu CN, Durraccio D, Gulumser G, Vasile C (2010) Preparation of stable acrylate/montmorillonite nanocomposite latex via in situ batch emulsion polymerization: Effect of clay types. Appl Clay Sci 49:288–297

Yoshioka M, Takabe K, Sugiyama J, Nishio Y (2006) Newly developed nanocomposites from cellulose acetate/layered silicate/poly (e-caprolactone): synthesis and morphological characterization. J Wood Sci 52:121–127